

## **Supporting Information**

### **Thermodynamic and Spectroscopic Analysis for Ammonia Absorption Mechanism of Borohydride System**

Zixin Xu,<sup>[a]</sup> Takahiro Ide,<sup>[a]</sup> Norio Ogita,<sup>[a]</sup> Shinsuke Ohyagi,<sup>[b]</sup> Takashi Wakabayashi,<sup>[b]</sup> Toru Hamanaka,<sup>[b]</sup> Higuchi Taisho,<sup>[b]</sup> Tomoyuki Ichikawa,<sup>[c]</sup> Fangqin Guo,<sup>\*,[a]</sup> Hiroki Miyaoka<sup>\*,[d]</sup> and Takayuki Ichikawa<sup>[a]</sup>

---

[a] Z. Xu, N. Ogita, F. Guo, T. Ichikawa  
Graduate School of Advanced Science and Engineering, Hiroshima University, 1-4-1 Kagamiyama,  
Higashi-Hiroshima 739-8527, Japan  
E-mail: (fang-qin-guo@hiroshima-u.ac.jp)

[b] S. Ohyagi, T. Wakabayashi, T. Hamanaka, H. Taisho  
KRI, Inc., 5-11-151 Torishima, Konohana, Osaka, 554-0051, Japan

[c] T. Ichikawa  
Hydrolabo Inc., 3-10-31 Kagamiyama, Higashi-Hiroshima, 739-0046, Japan

[d] H. Miyaoka  
Natural Science Center for Basic Research & Development, Hiroshima University, 1-3-1  
Kagamiyama, Higashi-Hiroshima 739-8530, Japan  
E-mail: (miyaoka@hiroshima-u.ac.jp)

# Contents

1. Experiments and Theoretical Calculations .....	3
2. Supporting PCI Figures .....	5
3. Thermodynamics Analysis .....	6
4. Raman Spectroscopy .....	7

## 1. Experiments and Theoretical Calculations

$\text{NaBH}_4$  (99.9% purity) and  $\text{LiBH}_4$  (99.9% purity) were purchased from Sigma-Aldrich Japan. To prevent moisture absorption and oxidation, all samples were handled in a glovebox (Miwa MDB-2BL) under purified argon.

Pressure-composition isotherm (PCI) measurements for  $\text{NH}_3$  absorption were conducted using BELSORP-HP-nex (pressure range:  $10^{-4}$  Pa to ammonia vapor pressure) and BELSORP-max (pressure range:  $10^{-8}$  Pa to atmospheric pressure) instruments (MicrotracBEL, Japan). In all the PCI results, the x-axis in the results is expressed in terms of the amount of  $\text{NH}_3$  absorbed per mole of absorbent, with units of mol/mol. The  $\text{LiBH}_4$  and  $\text{NaBH}_4$  powder were mixed with 1:1 molar ratio by hand milling using agate mortar and pestle for 5 minutes. To analyze the adsorption reactions of  $\text{LiBH}_4$  and  $\text{NaBH}_4$  with  $\text{NH}_3$ , conventional methods such as powder X-ray diffraction are limited due to the presence of liquid-phase intermediates and  $\text{NH}_3$  release during pressure reduction. To address this, *in-situ* spectroscopy was carried out under  $\text{NH}_3$  atmosphere conditions. The *in-situ* NMR measurements under ammonia ( $\text{NH}_3$ ) pressure were conducted using a Lambda500 spectrometer (JEOL Co. Ltd.) at a magnetic field strength of 11.7 T. The samples were put into high-pressure valved NMR tubes (Tokyo Chemical Industry Co., Ltd.), which is available for  $\text{NH}_3$  in pressure range from vacuum to 0.86 MPa. The chemical shifts were referenced to pure water at 4.21 ppm for  $^1\text{H}$ , to a saturated boric acid aqueous solution at 19.49 ppm for  $^{11}\text{B}$ , and to NaCl 1M solution at 7.21 ppm for  $^{23}\text{Na}$ , respectively. *In-situ* Raman spectroscopy was also performed under  $\text{NH}_3$  pressure, using indium seals resistant to  $\text{NH}_3$ . For the Raman measurements, a monochromatic laser (Spectra-Physics Stabilite2017,  $\lambda = 488$  nm) is focused on the samples, and quasi-backscattered light is collected. The light is directed to a spectrometer (Czerny-Turner grating spectrometer JASCO TSR-600/SH) via a lens and beam splitter, and then it is detected by a CCD (Princeton Instruments LN-1100PB) cooled by liquid nitrogen. Notably, these techniques exhibit complementary spectral behaviors: while NMR signals sharpen upon liquefaction due to increased molecular mobility, Raman peaks tend to broaden as the system transitions from a rigid solid to a disordered liquid. This contrast offers a powerful approach for cross-validating phase evolution across different states.

Geometric optimizations of  $\text{Li/NaBH}_4(\text{NH}_3)_n$  clusters ( $n = 0-7$ ) were performed using Gaussian 16 (Rev.C02 x86\_64 AVX2-enabled CPUs for Linux OS) at the conventional B3LYP/6-31+G(d,p) level to determine the lowest-energy configurations and support the experimental results. The energy calculations were conducted, and energy parameters were obtained through SHERMO post-processing.<sup>[25]</sup>

## 2. Supporting PCI Figures

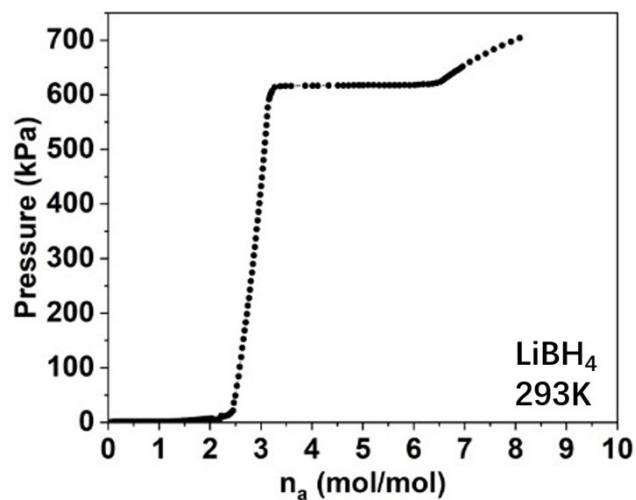


**Figure S1.** Full range PCI of  $\text{LiBH}_4$  at 293K.

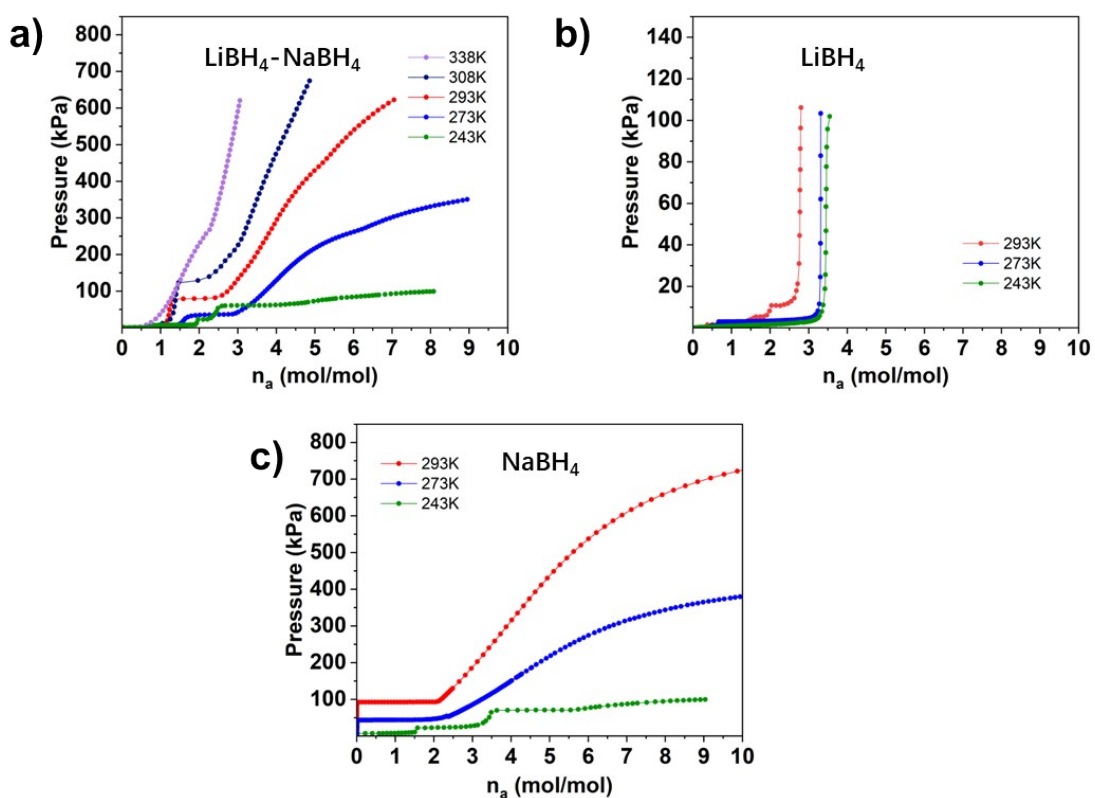


**Figure S2.** (a) Linear PCI Curves of 1:1  $\text{LiBH}_4$ - $\text{NaBH}_4$  mixture; (b) Linear PCI Curves of 1:1  $\text{LiBH}_4$ ; (c) Linear PCI Curves of 1:1  $\text{NaBH}_4$ .

### 3. Thermodynamics Analysis

Based on the plateau pressures (P) and experimental temperatures (T), the enthalpy change ( $\Delta H$ ) and entropy change ( $\Delta S$ ) of the corresponding reactions can be evaluated using the Van 't Hoff equation. Fig S2a and Fig S2b show the Van 't Hoff plots ( $\ln(p/p_0)$  vs  $T^{-1}$ ) for  $\text{LiBH}_4$  and the  $\text{LiBH}_4$ - $\text{NaBH}_4$  mixture, respectively. The slope and intercept of the vertical axis represent the values of  $\Delta H$  and  $\Delta S$ , respectively.

$$\ln \frac{P}{P_0} = \frac{\Delta H}{RT} - \frac{\Delta S}{R}$$

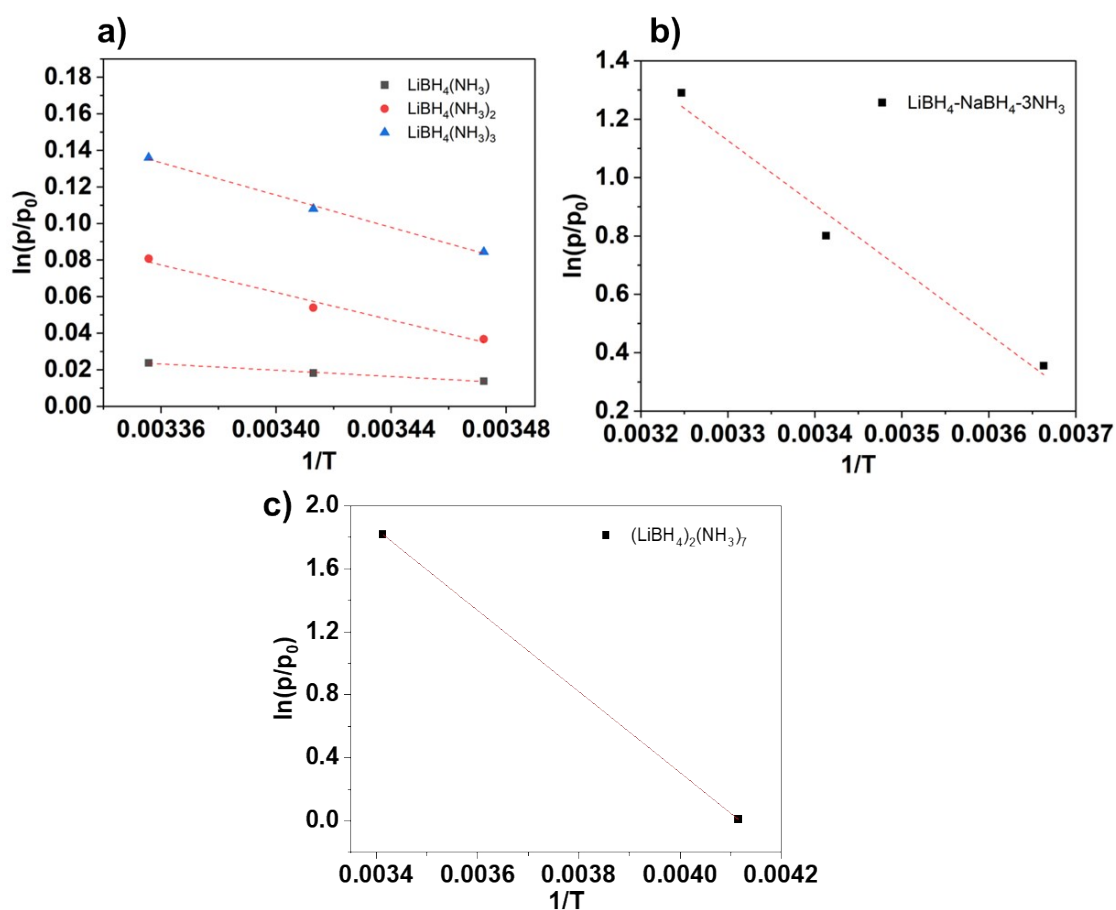


**Figure S3.** (a) Van't Hoff plots of  $\text{LiBH}_4$ ; (b) Van't Hoff plots of  $\text{LiBH}_4$ - $\text{NaBH}_4$ .

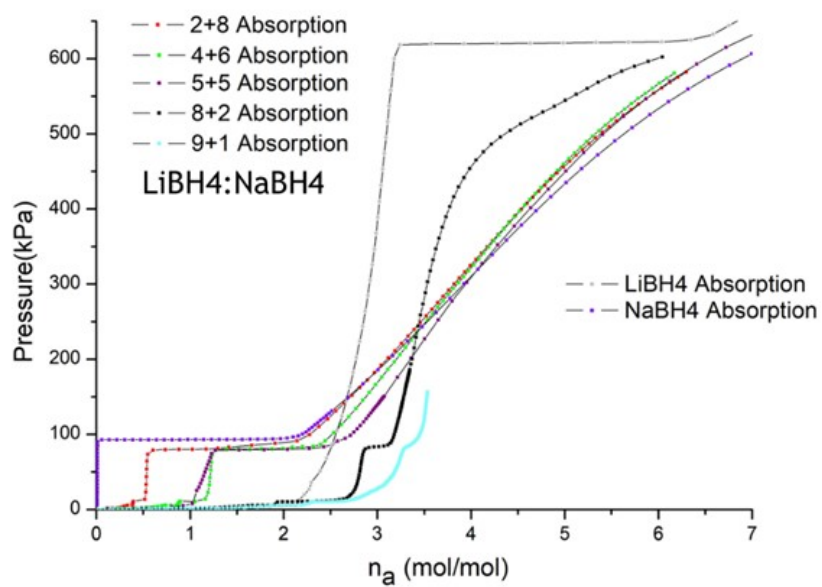


**Figure S4. PCI curves of  $\text{LiBH}_4$ – $\text{NaBH}_4$  mixtures with different  $\text{LiBH}_4$ : $\text{NaBH}_4$  ratios at 293K.**

#### 4. Raman Spectroscopy

To validate the analyses of coordination compounds and solutions, in-situ Raman spectroscopy measurements were conducted for  $\text{LiBH}_4$ ,  $\text{NaBH}_4$ , and the  $\text{LiBH}_4$ - $\text{NaBH}_4$  mixed system. All peaks observed in the results were thoroughly identified as shown in Table S1 and Table S2.<sup>[16–24]</sup> To avoid confusion, the peak nomenclature follows the conventions established in references.<sup>[18,19]</sup>

**Table S1.** Raman Peak Assignments of Pure  $\text{LiBH}_4$  and Pure  $\text{NaBH}_4$  at 293 K.

Materials	Vibration Mode	Symmetry	Wavenumber/ $\text{cm}^{-1}$	Note
$\text{LiBH}_4$	$\nu_4$	$A_g$	1098	B-H bending
	$\nu_4'$	$A_g$	1240	B-H bending
	$\nu_2$	$B_{3g}$	1289	B-H bending
	$\nu_2'$	$A_g$	1320	B-H bending
	$2\nu_4$	$A_g$	2156	Overtone of bending vibration $\nu_4$
	$\nu_3$	$A_g$	2274	B-H stretching
	$\nu_1$	$A_g$	2298	Tetrahedral B-H symmetric stretching
	$\nu_3'(\text{sh})$	$A_g$	2321	B-H stretching
$\text{NaBH}_4$	$\nu_4$	$F_2$	1127	B-H bending
	$\nu_2$	$A_1$	1279	B-H bending
	$2\nu_4$	$E_1$	2197	Overtone of bending vibration $\nu_4$
	$2\nu_4'$	$A_1$	2228	Overtone of bending vibration $\nu_4$
	$\nu_1$	$A_1$	2334	Tetrahedral B-H symmetric stretching



$\nu_2+\nu_4(\text{sh})$	E	2408	Combination band
$2\nu_2$	$A_1$	2541	Overtone of bending vibration $\nu_2$

\*sh=shoulder peak

**Table S2.** Raman Peak Assignments of  $\text{NH}_3$  in  $\text{LiBH}_4$  and  $\text{NaBH}_4$  after  $\text{NH}_3$  Absorption at 293 K.

Materials	Vibration Mode	Symmetry	Wavenumber/ $\text{cm}^{-1}$	Note
$\text{NH}_3$ ( $\text{LiBH}_4$ )	$\nu_{1(\text{sh})}$	$A_g$	3218	N-H stretching
	$\nu_2$	$E_g$	3293	N-H symmetric stretching
	$\nu_2^{\text{'}}$	$E_g$	3380	N-H stretching
$\text{NH}_3$ ( $\text{NaBH}_4$ )	$\nu_1$	$A_g$	3241	N-H stretching
	$\nu_2$	$E_g$	3301	N-H symmetric stretching
	$\nu_2^{\text{'}}$	$E_g$	3379	N-H stretching

\*sh=shoulder peak